



**HAL**  
open science

## Optimized process for the fabrication of PDMS membranes integrating permanent micro-magnet arrays

Lucie Descamps, Samir Mekkaoui, M.-C. Audry, A.-L. Deman, Damien Le Roy

### ► To cite this version:

Lucie Descamps, Samir Mekkaoui, M.-C. Audry, A.-L. Deman, Damien Le Roy. Optimized process for the fabrication of PDMS membranes integrating permanent micro-magnet arrays. *AIP Advances*, 2020, 10 (1), pp.015215. 10.1063/1.5129919 . hal-03229975

**HAL Id: hal-03229975**

**<https://hal.science/hal-03229975>**

Submitted on 27 May 2021

**HAL** is a multi-disciplinary open access archive for the deposit and dissemination of scientific research documents, whether they are published or not. The documents may come from teaching and research institutions in France or abroad, or from public or private research centers.

L'archive ouverte pluridisciplinaire **HAL**, est destinée au dépôt et à la diffusion de documents scientifiques de niveau recherche, publiés ou non, émanant des établissements d'enseignement et de recherche français ou étrangers, des laboratoires publics ou privés.

# Optimized process for the fabrication of PDMS membranes integrating permanent micro-magnet arrays

Cite as: AIP Advances **10**, 015215 (2020); <https://doi.org/10.1063/1.5129919>

Submitted: 04 October 2019 . Accepted: 30 November 2019 . Published Online: 10 January 2020

Lucie Descamps, Samir Mekkaoui, Marie-Charlotte Audry, Anne-Laure Deman, and Damien Le Roy

## COLLECTIONS

Paper published as part of the special topic on [64th Annual Conference on Magnetism and Magnetic Materials](#), [64th Annual Conference on Magnetism and Magnetic Materials](#) and [64th Annual Conference on Magnetism and Magnetic Materials](#)



View Online



Export Citation



CrossMark

## ARTICLES YOU MAY BE INTERESTED IN

[Anisotropic ferromagnetic polymer: A first step for their implementation in microfluidic systems](#)

AIP Advances **6**, 056604 (2016); <https://doi.org/10.1063/1.4943927>

[Micro-magnetic imprinting of high field gradient magnetic flux sources](#)

Applied Physics Letters **104**, 262401 (2014); <https://doi.org/10.1063/1.4886375>

[Synthesis of Nd-Fe-B/Fe hybrid micro-magnets](#)

AIP Advances **9**, 125139 (2019); <https://doi.org/10.1063/1.5130412>

Call For Papers!

AIP Advances

**SPECIAL TOPIC:** Advances in  
Low Dimensional and 2D Materials

# Optimized process for the fabrication of PDMS membranes integrating permanent micro-magnet arrays

Cite as: AIP Advances 10, 015215 (2020); doi: 10.1063/1.5129919

Presented: 6 November 2019 • Submitted: 4 October 2019 •

Accepted: 30 November 2019 • Published Online: 10 January 2020



View Online



Export Citation



CrossMark

Lucie Descamps,<sup>1,a)</sup> Samir Mekkaoui,<sup>1</sup> Marie-Charlotte Audry,<sup>1</sup> Anne-Laure Deman,<sup>1</sup> and Damien Le Roy<sup>2</sup>

## AFFILIATIONS

<sup>1</sup>Institut des Nanotechnologies de Lyon INL-UMR5270, CNRS, Université Lyon 1, Villeurbanne F-69622, France

<sup>2</sup>Institut Lumière Matière ILM-UMR 5306, CNRS, Université Lyon 1, Villeurbanne F-69622, France

**Note:** This paper was presented at the 64th Annual Conference on Magnetism and Magnetic Materials.

<sup>a)</sup>E-mail: [lucie.descamps@univ-lyon1.fr](mailto:lucie.descamps@univ-lyon1.fr)

## ABSTRACT

Here we report on the fabrication of micro-magnet arrays by powder agglomeration in a polymer matrix. The NdFeB@polydimethylsiloxane (PDMS) inner microstructure and the generated magnetic forces were studied, when prepared under two different magnetic field configurations. The initial process uses the classical crosslinking of PDMS mixed with NdFeB powder under a low magnetic field gradient provided by a permanent magnet (LG set-up for low gradient). In contrast, the optimized process uses an intermediate layer, composed of iron microstructures in a PDMS matrix that amplifies and focuses the magnetic field gradient given by the permanent magnet (HG set-up for high gradient). Both processes result in a heterogeneous material that can be described as an array of permanent micro-magnets diluted in a non-magnetic host matrix. The NdFeB@PDMS microstructure was characterized by X-ray tomography and optical microscopy. The magnetic properties were also measured by magnetometry and colloidal probe AFM. Results showed that the HG set-up leads to an array of micro-magnets localized at the surface, with higher compactness and density, resulting in stronger magnetic performances compared to the LG set-up. This technology only implies easy-to-handle and cheap fabrication processes, paving the way for the development of low-cost lab-on-chip devices integrating magnetophoretic trapping functionality.

© 2020 Author(s). All article content, except where otherwise noted, is licensed under a Creative Commons Attribution (CC BY) license (<http://creativecommons.org/licenses/by/4.0/>). <https://doi.org/10.1063/1.5129919>

## I. INTRODUCTION

Contactless actuation and manipulation through magnetic force can serve to perform a large panel of functionalities in microsystems (Arnold and Wang, 2009), including microvalves (Oh and Ahn, 2006 and Nakahara *et al.*, 2018), energy harvesters (Wang *et al.*, 2013), micro-undulators (Peterson *et al.*, 2014), or cells sorting (Chen *et al.*, 2013; Alam *et al.*, 2018; and Shen *et al.*, 2019). In more fundamental biomedical studies, magnetic forces appear as an efficient means to mediate local mechanical stimuli on cells (Kim *et al.*, 2010 and Bidan *et al.*, 2018) and micro-organisms (Mittrossilis *et al.*, 2017).

As compared to other approaches, systems' downscaling is beneficial to the intensity of the magnetic force. Indeed, the force scaling with the magnetic field gradient, the smaller the magnetic

field source the larger the reachable force (Cugat *et al.*, 2003). Inevitably, this reduces the interaction distance. The best compromise in microsystems would often be a large density of 5-50  $\mu\text{m}$  size micromagnets.

In the literature, micro-magnets generally refer, without distinction, to magnetically-soft or-hard micropatterns, both approaches enabling strong magnetic field values (a fraction of one Tesla). Soft micropatterns, made of Ni, Ni-Fe, are certainly the most commonly used. They can serve to produce a large modulation of the magnetic field at the micrometer scale by locally focusing the flux lines of an external magnet (Arnold *et al.*, 2004; Huang *et al.*, 2015; Ko *et al.*, 2016; and Mekkaoui *et al.*, 2018). In contrast, magnetically-hard micro-patterns, notably made of L1<sub>0</sub>-FePt (Overweg *et al.*, 2015), L1<sub>0</sub>-CoPt (Wang and Arnold, 2008 and Oniku *et al.*, 2014), NdFeB (Wang *et al.*, 2008 and Dumas-Bouchiat

*et al.*, 2010),  $\text{SmCo}_5$  (Walther *et al.*, 2009), permit autonomous operation as they generate their own stray magnetic field and gradient at remanence state.

Permanent micro-magnets of less than  $100\ \mu\text{m}$  have been successfully prepared from discontinuous films, either topographically patterned using pre-etched substrates (Zablotskii *et al.*, 2013), photoresist molds (Wang and Arnold, 2008), or locally reversing the magnetization (Dumas-Bouchiat *et al.*, 2010 and Garraud *et al.*, 2014). Film-based techniques led to precise control over the shape, size, reproducibility, material microstructure and texture (Le Roy *et al.*, 2016a). However, they rely on relatively complex and expensive microfabrication processes. Besides, the off-equilibrium film growth conditions require post-deposition heat treatments at elevated temperatures to form the high magnetocrystalline anisotropy phase (Dempsey *et al.*, 2007 and Fujiwara *et al.*, 2018). This complicates the integration in microsystems, notably in polymer-based devices. A cheap and simple alternative consists of resin-bonded micromagnets (Wang *et al.*, 2013). Magnetically-hard powder is mixed with polymer and deposited in molds (Oniku *et al.*, 2013). In order to scale down the magnet size to a few tens of micrometers, it was proposed to precisely position the hard micro-particles within the polymer matrix using a magnetically-patterned film (Dempsey *et al.*, 2014). However, the master structures to replicate were prepared using relatively complex micro-fabrication routes. Besides, the geometry of the template led to line agglomerates, while, in the context of cells trapping in microfluidic devices, arrays of dot-like micro-magnets could permit to trap large densities of individual cells.

Here we report on an optimized process to form arrays of micrometer-sized permanent magnets by only employing easy-to-handle and cheap fabrication methods. These permanent magnets made of NdFeB micro-particle agglomerates present high remanence and large coercive fields. Several characterizations have been performed to compare the morphology and the performances obtained from both processes: X-ray tomography, optical, SQUID magnetometer and magnetic force measurements with colloidal AFM probes.

## II. EXPERIMENTAL

### A. Composite preparation

A mixture containing NdFeB micro-particles and uncured PDMS (10/1 w/w of monomer and curing agent, respectively) (Sylgard from Samaro) was thoroughly stirred in a mortar (around

4 min) until obtaining a homogeneous material prior to polymer cross-linking. Used NdFeB micro-particles are irregularly shaped crushed melt-spun ribbon (MQFP-B,  $0.5\text{--}7\ \mu\text{m}$  size) provided by Magnequench International, Inc. According to the supplier's datasheet, the remanent magnetic flux,  $B_r$ , and the coercive field,  $H_c$ , are of 0.9 T and 740 kA/m, respectively. We investigated NdFeB@PDMS composites with concentrations of 1 wt% NdFeB. In the same way, composites made of iron powder (dry powder,  $0.5\text{--}7\ \mu\text{m}$  diameter, 97% Fe basis, Sigma-Aldrich) and designated as i-PDMS were prepared at 7.5wt%.

### B. Microstructuration - « low » and « high » magnetic field gradient set-up

NdFeB@PDMS microstructures were obtained according to an already described method for i-PDMS (Mekkaoui *et al.*, 2018). Briefly, the NdFeB@PDMS membrane was molded in a  $100\text{-}\mu\text{m}$ -thick Kapton adhesive film, cut by Xurography (Renaud *et al.*, 2015), and stuck to a substrate. The membrane was then cured at  $70^\circ\text{C}$  for 2h in a magnetic field of 300 mT supplied by a bulk NdFeB magnet ( $60 \times 30 \times 15\ \text{mm}^3$ , magnetization along the shortest dimension). During curing, NdFeB particles are free to move in the liquid polymer and self-organize driven by magnetic forces. After curing, NdFeB particles are immobilized in the polymer matrix. The Kapton mold was then removed leaving a  $100\text{-}\mu\text{m}$ -thick composite layer and pure PDMS was poured on it in order to increase the thickness up to 1 mm. The membrane was then cured at  $70^\circ\text{C}$  for 2 hours and peeled off from the glass slide. Finally, NdFeB@PDMS microstructures were magnetized using a magnetizing system producing a field of  $\sim 1\ \text{T}$ . All the fabrication steps are summarized in Figure 1.

In the initial process, the substrate on which the NdFeB is molded is a silanized glass slide. During the crosslinking step, the composite membrane is only submitted to the magnetic field gradient generated by the external magnet, estimated at 20 T/m from numerical simulations (Comsol Multiphysics®). In contrast, in the optimized process, the substrate is an i-PDMS template containing chain-like agglomerates of Fe microparticles, oriented in the direction perpendicular to the substrate's surface. The agglomerates are characterized by an average size of  $7.5\ \mu\text{m}$  in the plane and an areal density of 1500 agglomerates/ $\text{mm}^2$ . In this configuration, strong magnetic field gradients are generated locally, at the chain positions. They were estimated from numerical simulations (Comsol Multiphysics®) and magnetic field gradient values as high as  $10^5\ \text{T/m}$  at a distance of  $1\ \mu\text{m}$  from the surface of the

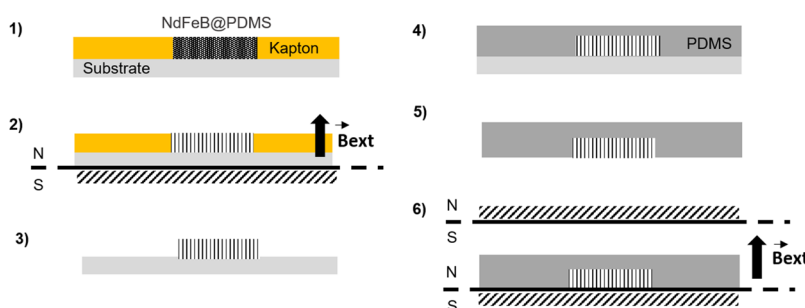


**FIG. 1.** Fabrication steps of the NdFeB@PDMS composite. The composite is molded in a Kapton film bonded to a substrate. The substrate is either a silanized glass slide for LG set-up or an i-PDMS template for HG set-up. The composite is then placed in a 300 mT magnetic field for NdFeB particles self-organization in chains (step 2). The Kapton mold is then removed and pure PDMS is poured on the membrane (steps 3-4). Finally, after curing at  $70^\circ\text{C}$  for 2h, the composite membrane is peeled off (step 5) and magnetized under a magnetic field of 1 T (step 6).

i-PDMS medium were calculated. Thus, the magnetic field gradient is 5000 times larger when the i-PDMS membrane is used. The initial process and the optimized process are respectively referred to as low gradient set-up (LG set-up), and high gradient set-up (HG set-up) in the following discussion.

### C. Characterization methods

The influence of LG and HG set-ups on the NdFeB@PDMS structure and magnetism was investigated. The inner structure was first characterized by X-ray tomography, using the EasyTomNano  $\mu$ CT tomograph (RX Solutions). The X-ray source is a LaB<sub>6</sub> cathode with a diamond window leading to higher flux (20  $\mu$ A). Its focal spot measures 0.25  $\mu$ m and a tension of 90 kV was applied. Scans were acquired by a CCD detector, whose matrix measures 2000 x 1312 pixels, with a resolution of 0.3  $\mu$ m. 3D images were reconstructed from projections at 1400 different angular positions. Final images of 1700 x 1700 x 400 voxel, i.e 510x510x120  $\mu$ m<sup>3</sup>, were obtained and processed with ImageJ to characterize NdFeB particles' spatial organization in the volume of the composite membrane. Conventional optical microscopy characterizations using an Olympus BX51M microscope coupled to a camera (Moticam2000, Motic) were also carried out with ImageJ to study the in-plane organization of the NdFeB agglomerates. Concerning the magnetic properties, magnetization and demagnetization processes were measured in a SQUID magnetometer. In order to investigate the magnetic performances in the context of magnetophoretic trapping, magnetic force measurements were carried out on the AFM MFP-3D (Asylum Research, Oxford Instrument) using superparamagnetic colloidal probes. The acting force between the colloid and the sample was recorded as the probe approached and withdrew from the sample surface.

## III. RESULTS AND DISCUSSION

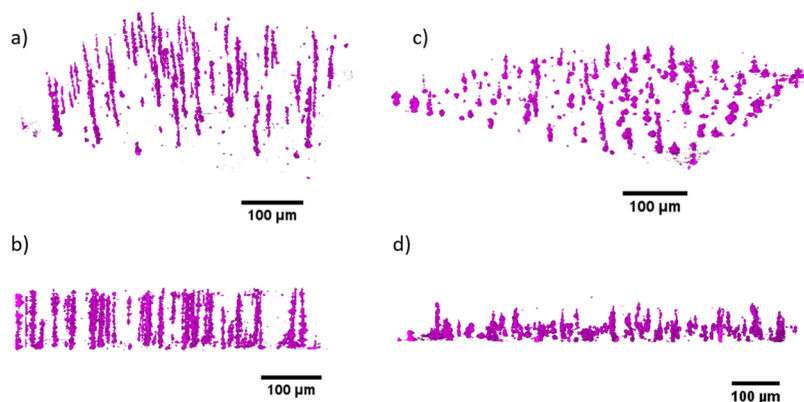
### A. Structural characterization

Figure 2 displays reconstructed 3D profiles from X-ray tomography performed on a volume of 510 x 510 x 120  $\mu$ m<sup>3</sup>. For both LG and HG set-ups, tomography images revealed two types of organizations: chain-like agglomerates (CA), and also isotropic agglomerates (IA), of sizes less than 7  $\mu$ m. Proportions of CA and IA depend

on the used configuration. Indeed, with the LG set-up, CA structures are predominant (75%). In contrast, with HG set-up, nearly the same proportion of CA and IA were observed, 53% and 47% respectively. In addition, the magnetic field gradient modifies the CA morphology. With HG set-up, the length of CA is about four times shorter than that of CA obtained with LG set-up. The length measures about 18  $\mu$ m for HG set-up and 84  $\mu$ m for LG set-up. Moreover, one can notice that the CA not only have a shorter length but also present a conical shape. The compactness of microstructures was also investigated by studying the spacing between NdFeB particles in the agglomerates. With the LG set-up, for 2/3 of agglomerates' number, the particles are spaced by a distance larger than 300 nm (the pixel size in tomography), while it is the case for only 1/3 of them with the HG set-up. Considering the distribution of the particles within the matrix, one can clearly observe that the agglomerates are either elongated throughout the entire membrane thickness (LG set-up) or concentrated on one side of the membrane (HG set-up).

To summarize the tomography results, the HG set-up leads to micro-magnets with a shorter length and higher compactness, located closer to the NdFeB@PDMS surface, as compared to the ones obtained with the initial LG set-up. This can be explained by the agglomeration mechanism during the PDMS crosslinking, in which two magnetic interactions come into play (Le Roy *et al.*, 2016b): (i) the magnetic dipole-dipole interaction, that gathers the particles and tends to align their magnetic moments ( $m$ ), (ii) the magnetic interaction between the dipole and the surrounding magnetic field, that attracts the particle towards the region of maximum magnetic field. The magnitudes of the two corresponding forces are strongly affected by the substrate introduced between the external magnet and the uncured PDMS as it deeply modifies the external field distribution.

As described in Figure 3, in the LG set-up, the substrate is simply a silanized glass slide, and the composite membrane is submitted to the magnetic vertical gradient of the bulk magnet. In this case, the chain formation is mostly due to the dipole-dipole interaction (Fragouli *et al.*, 2010 and Tracy and Crawford, 2013) with a slight attraction towards the glass surface. Using the HG set-up, the substrate is a silanized i-PDMS template, in which iron microstructures concentrate the magnetic flux lines and permit to achieve larger magnetic field gradients than that of the LG set-up. This time, the



**FIG. 2.** Reconstructed views from X-ray tomography performed on a volume of 510 x 510 x 120  $\mu$ m<sup>3</sup> of one representative membrane at 1 wt%. (a,c) 3D view for LG and HG configurations, respectively. (b,d) Projections on XZ plane, for LG and HG configurations, respectively.

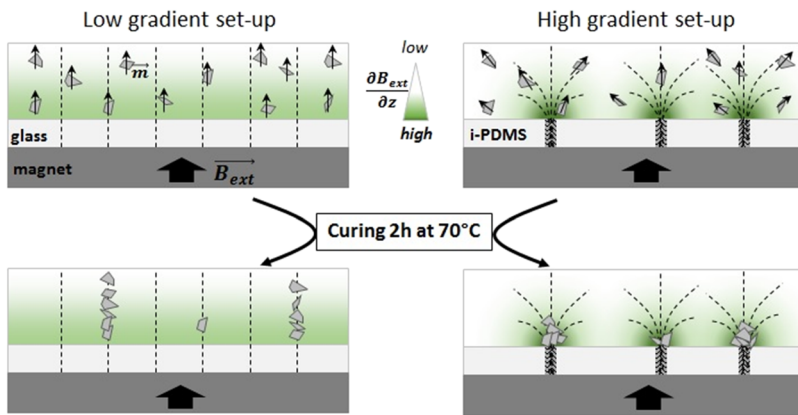


**FIG. 3.** Sketch of the chain formation mechanism for both LG and HG set-up. While in the LG set-up the chain formation is mainly due to the dipole-dipole interaction, in the HG set-up the chain formation is due to both dipole-dipole and dipole-magnetic field interactions. It depends on the substrate which modifies the external magnetic field distribution.

chain formation is due to both dipole-dipole and dipole-magnetic field interactions, the latter producing a strong attraction of the particles towards the template surface.

The aforementioned forces are obviously in competition with the viscous force (Ghosh and Puri, 2013 and Marchi *et al.*, 2015) that counteracts the NdFeB particles motion. As the crosslinking proceeds, the particles are less and less mobile until complete immobilization.

These NdFeB microstructures, once magnetized, will work as micro-magnets. Using optical microscopy at a magnification of  $\times 100$ , we have characterized the magnetic array's properties such as the density of the micro-magnets, nearest neighbor distance, and diameter. Figure 4 shows top view images of the micro-magnet arrays, at a magnification of  $\times 100$ . Using HG set-up, there is a larger number of micro-magnets with an average density of 740 magnets/ $\text{mm}^2$ , against 480 magnets/ $\text{mm}^2$  with the LG set-up. The i-PDMS template allowed NdFeB particles to spread in the PDMS matrix and therefore increases the micro-magnets density by a factor 1.5. As a consequence, the average nearest neighbor distance is inferior for arrays obtained with HG set-up. It is about  $25 \mu\text{m}$ , while it equals  $32 \mu\text{m}$  for LG set-ups. With both magnetic configurations, micrometer-sized magnets with a diameter of around  $6 \mu\text{m}$  were obtained. The resulting material can be implemented as an array of magnetic micro-traps in microsystems.

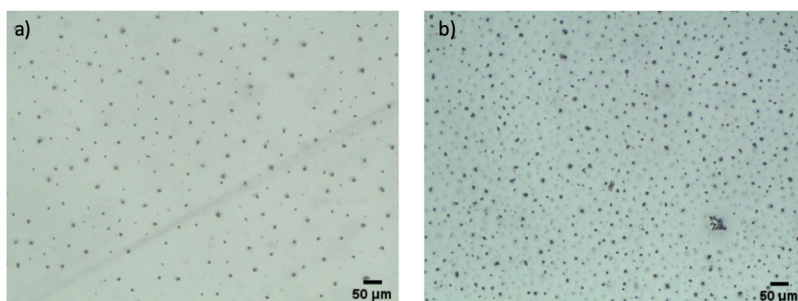
## B. Magnetic characterization

Figure 5 shows room temperature magnetization curves measured by SQUID magnetometry. Micro-magnets prepared with

HG and LG set-ups (Figure 5a) exhibit superimposed magnetization curves. Thus the drastic difference in the agglomerates' shape obtained using the two set-ups and revealed by X-ray tomography does not influence the magnetization process. This can be expected considering the high magnetic hardness parameter ( $\kappa = 1.54$ ) of the  $\text{Nd}_2\text{Fe}_{14}\text{B}$  phase (Coey, 2011). Magnetization curves measured either parallel or perpendicular to the long axis of the agglomerates referred to as out-of-plane (oop) and in-plane (ip), respectively, are shown in figure 5b. The oop curve shows a slightly larger squareness than the ip curve, revealing an easy direction for the magnetization along the agglomerates' orientation. This could then be attributed to a preferential alignment of the  $\text{Nd}_2\text{Fe}_{14}\text{B}$   $c$ -axes during the formation of the microparticle agglomerates along the applied field direction. This is however limited as the polycrystalline microparticles are poorly textured. The relatively small kink at low fields could be the sign of a secondary and magnetically soft phase, which might be due to surface oxidation.

## C. Magnetic force measurements by colloidal probe AFM

The AFM force measurements have been performed with a  $14\text{-}\mu\text{m}$ -diameter superparamagnetic bead (product average diameter:  $12 \mu\text{m}$ , density:  $1.1 \text{ g/cm}^3$ , magnetization:  $0.55 \text{ kA/m}$ , material: magnetite nano-inclusions in a polystyrene matrix, Kisker<sup>®</sup>) glued to a silicon nitride cantilever (PNP-TR-TL, NanoAndMore, stiffness  $43 \text{ pN/nm}$ ) in a  $10 \text{ mM NaCl}$  solution so as to screen electrostatic forces. In this case, the superparamagnetic bead is submitted



**FIG. 4.** Brightfield microscopy images of an array of micro-magnets obtained with both configurations: a) LG set-up and b) HG set-up.

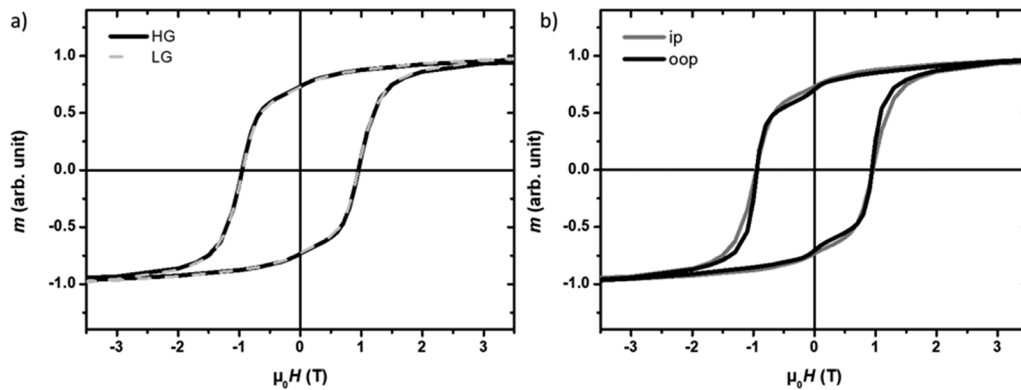


**FIG. 5.** Room temperature magnetization curves of 1wt% NdFeB@PDMS membranes. (a) Comparison of the in-plane magnetization curves for membranes prepared with “high gradient set-up” (HG) and “low gradient set-up” (LG). (b) Comparison of the in-plane (ip) and out-of-plane (oop) magnetization for a HG-prepared membrane.

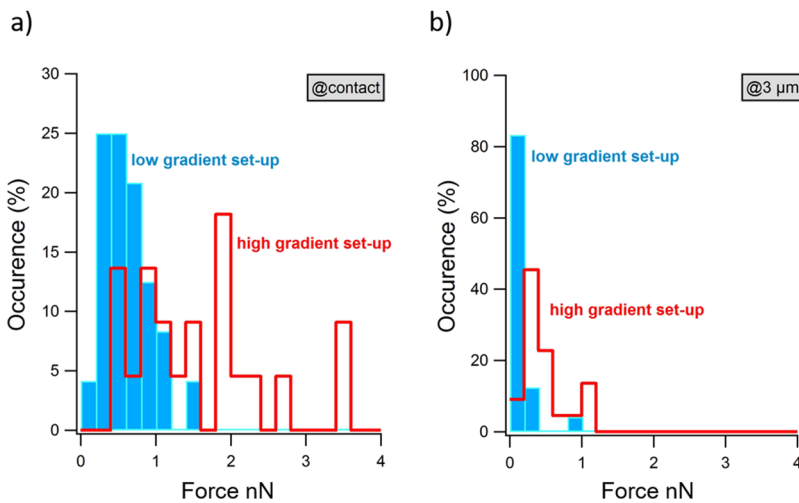


**FIG. 6.** Measured magnetic forces by colloidal probe AFM. (a) Force in contact with the composite surface for LG and HG set-ups. (b) Force at a 3- $\mu\text{m}$  distance from the surface for LG and HG set-ups.

to an attractive force proportional to the magnetic field gradient. Micro-magnets act as traps and give straight information about the capture performance. AFM approach and retract curves were performed on about 20 micro-magnets for each sample preparation. Figure 6 presents magnetic force magnitudes when the bead is at contact with the surface of the NdFeB@PDMS membrane or at a distance of 3  $\mu\text{m}$ . For the sample obtained with the LG set-up, the contact force ranges from 0.1 to 1.4 nN while for the HG sample, it reaches 3.6 nN. In addition, the average contact force for HG microstructures is almost three times larger than that of LG microstructures (1.7 nN and 0.6 nN, respectively). Regarding the magnetic force's range, AFM measurements reveal that a majority of the LG microstructures generates magnetic forces between 0.1 and 0.2 nN at a distance of 3  $\mu\text{m}$  from their surface, while magnetic forces reach 0.3–0.5 nN for HG microstructures, which is twice as great as LG magnetic force range. Therefore, the use of an i-PDMS membrane during the NdFeB@PDMS composite curing has a substantial positive impact on the magnetic forces of the latter. This could be attributed to the combined effects of larger compactness, resulting in less magnetic flux loss and a higher concentration of magnetic

particles at the surface. The measured forces are relatively intense, about a few nN, as compared to the ones usually encountered in microfluidic devices, in the order of a few pN (Zhou *et al.*, 2016 and Jaiswal *et al.*, 2017).

#### IV. CONCLUSION

We have presented an optimized method to fabricate arrays of micrometer-sized permanent magnets. It rests on a cheap and easy-to-handle fabrication process consisting of mixing a NdFeB magnetic powder with PDMS. These permanent magnets present high remanence and large coercive fields. As compared to the initial process, the use of i-PDMS template permits to create enhanced local magnetic field gradients, during the NdFeB@PDMS preparation. This results in larger density arrays of more compact micro-magnets. This optimized route leads to higher reachable magnetic forces, as well as a longer interaction range. This novel approach could be easily used to integrate micro-magnets in microsystems, thus developing autonomous and compact magnetophoretic trapping devices.

## ACKNOWLEDGEMENTS

The work was financially supported by the Auvergne-Rhône-Alpes region (Pack Ambition Recherche 2017 – LUTON project). We wish to acknowledge support for the project from Nanolyon technological platform, MATEIS lab for X-ray tomography measurements, and ILM-Tech for AFM and SQUID facilities.

## REFERENCES

- Alam, M. K., Koomson, E., Zou, H., Yi, C., Li, C.-W., Xu, T., and Yang, M., *Analytica Chimica Acta* **1044**, 29–65 (2018).
- Arnold, D. P., Zana, I., Cros, F., and Allen, M. G., *IEEE Trans. on Magn.* **40**(4), 3060–3062 (2004).
- Arnold, D. P. and Wang, N., *J. Microelectromech. Syst.* **18**(6), 1255–1266 (2009).
- Bidan, C. M., Fratzl, M., Coullomb, A., Moreau, P., Lombard, A. H., Wang, I., Balland, M., Boudou, T., Dempsey, N. M., Devillers, T., and Dupont, A., *Scientific Reports* **8**, 1464 (2018).
- Chen, P., Huang, Y.-Y., Hoshino, K., and Zhang, X., *Lab Chip* **14**(3) (2013).
- Coe, J. M. D., *IEEE Trans. on Magn.* **47**(12), 4671–4681 (2011).
- Cugat, O., Delamare, J., and Reyne, G., *IEEE Trans. on Magn.* **39**, 3608 (2003).
- Dempsey, N. M., Walther, A., May, F., Givord, D., Khlopkov, K., and Gutfleish, O., *Appl. Phys. Lett.* **90**, 092509 (2007).
- Dempsey, N. M., Le Roy, D., Marelli-Mathevon, H., Shaw, G., Dias, A., Kramer, R. B. G., Le Viet, C., Kustov, M., Zanini, L. F., Villard, C., Hasselbach, K., Tomba, C., and Dumas-Bouchiat, F., *Applied Physics Letters* **104**, 262401 (2014).
- Dumas-Bouchiat, F. *et al.*, *Appl. Phys. Lett.* **96**(10), 102511 (2010).
- Fragouli, D., Buonsanti, R., Bertoni, G., Sangregorio, C., Innocenti, C., Falqui, A., Gatteschi, D., Cozzoli, P. D., Athanassiou, A., and Cingolani, R., *ACS Nano* **4**(4), 1873–1878 (2010).
- Fujiwara, R., Devillers, T., Givord, D., and Dempsey, N. M., *AIP Advances* **8**, 056225 (2018).
- Garraud, A., Oniku, O. D., Patterson, W. C., Shorman, E., Le Roy, D., Dempsey, N. M., Arnold, D. P., *2014 IEEE 27th International Conference on Micro Electro Mechanical Systems (MEMS)* (MEMS, 2014).
- Ghosh, S. and Puri, I. K., *Soft Matter* **9**, 2024 (2013).
- Huang, Y. Y., Chen, P., Wu, C.-H., Hoshino, K., Sokolov, K., Lane, N., Liu, H., Huabschman, M., Frenkel, E., and Zhang, J. X. J., *Scientific Reports* **5**, 16047 (2015).
- Jaiswal, D., Rad, A. T., Nieh, M. P., Claffey, K. P., and Hoshino, K., *J. Magn. Mater.* **427**, 7–13 (2017).
- Kim, D.-H., Rozhkova, E. A., Ulasov, I. V., Bader, S. D., Rajh, T., Lesniak, M. S., and Novosad, V., *Nat. Mater.* **9**(2), 165–171 (2010).
- Ko, J., Yelleswarapu, V., Singh, A., Shah, N., and Issadore, D., *Lab. Chip.* **16**(16), 3049–3057 (2016).
- Le Roy, D., Shaw, G., Haettel, R., Hasselbach, K., Dumas-Bouchiat, F., Givord, D., and Dempsey, N. M., *Materials Today Communications* **6**, 50–55 (2016a).
- Le Roy, D., Dhungana, D., Ourry, L., Faivre, M., Ferrigno, R., Tamion, A., Dupuis, V., Salles, V., and Deman, A.-L., *AIP Adv* **6**(5) (2016b).
- Marchi, S., Casu, A., Bertora, F., Athanassiou, A., and Fragouli, D., *ACS Appl. Mater. Interfaces* **7**, 19112 (2015).
- Mekkaoui, S., Le Roy, D., Audry, M.-C., Lachambre, J., Dupuis, V., Desgouttes, J., and Deman, A.-L., *Microfluidics and Nanofluidics* **22**, 119 (2018).
- Mittrossilis, D., Röper, J. C., Le Roy, D., Driquez, B., Michel, A., Ménager, C., Shaw, G., Le Demnat, S., Ranno, L., Dumas-Bouchiat, F., Dempsey, N. M., and Farge, E., *Nature Communications* **8**, 13883 (2017).
- Nakahara, T., Suzuki, J., Hosokawa, Y., Shimokawa, F., Kotera, H., and Suzuki, T., *Magnetochemistry* **4**, 7 (2018).
- Oh, K. W. and Ahn, C. H., *J. Micromech. Microeng.* **16**, R13–R39 (2006).
- Oniku, O. D., Bowers, B. J., Shetye, S. B., Wang, N., and Arnold, D. P., *J. Micromech. Microeng.* **23**(7), 075027 (2013).
- Oniku, O. D., Qi, B., and Arnold, D. P., *J. Appl. Phys.* **115**(17), 17E521 (2014).
- Overweg, H. C., den Haan, A. M. J., Eerkens, H. J., Alkemade, P. F. A., La Rooij, A. L., Spreeuw, R. J. C., Bossoni, L., and Oosterkamp, T. H., *Appl. Phys. Lett.* **107**, 072402 (2015).
- Peterson, B. A., Oniku, O. D., Patterson, W. C., Le Roy, D., Garraud, A., Herrault, F., Dempsey, N. M., Arnold, D. P., and Allen, M. G., *Physics Procedia* **52**, 36–45 (2014).
- Renaud, L., Selloum, D., and Tingry, S., *Microfluid Nanofluid* **18**, 1407 (2015).
- Shen, Y., Yalikhun, Y., and Tanaka, Y., *Sensors and Actuators B: Chemical* **282**, 268–281 (2019).
- Tracy, J. and Crawford, T., *MRS Bulletin* **38**(11), 915–920 (2013).
- Walther, A. *et al.*, *J. Magn. Mater.* **321**(6), 590–594 (2009).
- Wang, N. and Arnold, D. P., *IEEE Trans. on Magn.* **44**(11), 3969–3972 (2008).
- Wang, N., Bowers, B. J., and Arnold, D. P., *J. Appl. Phys.* **103**(7), 07E109 (2008).
- Wang, P.-H., Tao, K., Yang, Z.-Q., and Ding, G.-F., *J. Zhejiang Univ-Sci C (Comput & Electron)* **14**(4), 283–287 (2013).
- Zablotskii, V., Dejneka, A., Kubinova, S., Le Roy, D., Dumas-Bouchiat, F., Givord, D., Dempsey, N. M., and Sykova, E., *PLoS ONE* **8**(8), e70416 (2013).
- Zhou, R., Yang, Q., Bai, F. *et al.*, *Microfluid Nanofluid* **20**, 110 (2016).